Infant skull fractures: Accident or abuse?
Evidences from biomechanical analysis using finite element head models

Xiaogai Li[a,*], Håkan Sandler[b,c], Svein Kleiven[a]

[a] Division of Neuronic Engineering, School of Technology and Health, Royal Institute of Technology - KTH, Huddinge 141 52, Sweden
[b] Department of Surgical Sciences/Forensic Medicine, Uppsala University, Uppsala, Sweden
[c] National Board of Forensic Medicine, Uppsala, Sweden

A R T I C L E   I N F O

A B S T R A C T

Abusive Head Trauma (AHT) is considered by some authors to be a leading cause of traumatic death in children less than two years of age and skull fractures are commonly seen in cases of suspected AHT. Today, diagnosing whether the observed fractures are caused by abuse or accidental fall is still a challenge within both the medical and the legal communities and the central question is a biomechanical question: can the described history explain the observed fractures? Finite element (FE) analysis has been shown a valuable tool for biomechanical analysis accounting for detailed head geometry, advanced material modelling, and case-specific factors (e.g. head impact location, impact surface properties). Here, we reconstructed two well-documented suspected abuse cases (a 3- and a 4-month-old) using subject-specific FE head models. The models incorporate the anatomical details and age-dependent anisotropic material properties of infant cranial bones that reflect the grainy fibres radiating from ossification centres. The impact locations are determined by combining multimodality images. The results show that the skull fracture patterns in both cases of suspected abuse could be explained by the described accidental fall history, demonstrating the inherent potential of FE analysis for providing biomechanical evidence to aid forensic investigations. Increased knowledge of injury mechanisms in children may have enormous medico-legal implications world-wide.

© 2018 Published by Elsevier B.V.

1. Introduction

There is a controversy in how to determine whether injuries to infants are due to accident or abuse. Several studies suggest that when skull fractures, especially multiple fractures, bilateral fractures, and fractures with complex configuration are present, child abuse should be suspected [1,2]. Experimental studies by Weber [3] indicated that a single impact to the head could cause multiple skull fractures; in practice, however, when pathologists and clinicians observe multiple skull fractures, the question of non-accidental origin will almost always be raised. Abusive Head Trauma (AHT) (formerly referred to as Shaken Baby Syndrome) is recommended to be defined as violent shaking only or combined with blunt impact, causing serious head injuries such as subdural hematoma, retinal haemorrhage, brain edema, and skull fractures [4].

AHT is considered by some authors to be a leading cause of traumatic death in children less than two years of age [5], and population-based studies of AHT suggest an incidence ranging from 14 to 40 per 100,000 children in infants less than 1 year of age [6]. In US, it's estimated that about 30 children younger than one year of age per 100,000 are injured from AHT, resulting in at least 1200 seriously injured infants and at least 80 deaths each year [7]. Further, younger age has a higher risk of death due to maltreatment and the peak age categories are 0–3 months (25%) and 2–6 years (19%) according to a survey study of 162 child fatality cases [8]. A Canadian study suggests that a minimum of 40 cases of AHT occur in Canada annually, with a mortality rate of almost 20% [9]. The economic cost of AHT is substantial [10,11], not to mention the life-long tragedies for the victims of the youngest children behind the number of each case. Many cases of AHT go unrecognized, resulting in further maltreatment and in some cases death, as stated in an early study [12]. Meanwhile, there are thousands of families are torn apart each year due to wrongful convictions to the innocent parents and caretakers. In particular, skull fractures are commonly seen both in cases of suspected AHT as well as accidental fall [13–21] and diagnosing whether the observed skull

fractures are caused by non-accidental or accidental fall challenges the medico-legal practitioners [13,22,23].

To understand the etiology of infant skull fracture due to falls, Weber [3,24] dropped infant post mortem human subjects (PMHS) from a height of 82 cm onto surfaces of different stiffness at the occipital-parietal lobe and depicted the skull fracture patterns. All drops onto stiff tile floor resulted in simple linear fractures. Weber's study, being the first systematic study of fracture mechanisms in infant cadavers, is still quite often referred to by the forensic investigators nowadays. Considering ethical concerns and limited availability of human specimens, experimental studies using infant porcine specimens have also been performed [25–29], these studies provide valuable information to help understand human infant skull fracture biomechanics and patterns. Parallel to the experimental efforts, numerical approaches especially the FE method allows accounting for detailed geometry, advanced material properties and complex boundary conditions and have been a powerful tool to study head injuries in general [30–36] as well as attempted efforts to study human infant skull fractures [37,38]. Anthropomorphic infant surrogates have also played an important role in understanding head kinematics during low height falls [39].

A variety of specificity of skull fractures seen from radiological images has been proposed for child abuse, e.g. multiple and complicated skull fractures with fracture width >3 cm [22,40]; bilateral fracture [23]; it is also suggested that a child abuse is likely when in lesions of average or low specificity there is no explanation for the cause of the trauma or when the explanation does not correspond with the nature of the trauma [23]. Another example, the most prevalent skull fracture in abuse is unilaterally localised, simple linear fracture of the parietal bone without depression. However, this also happens to be the most prevalent fracture patterns in accidents [13]. Most skull fractures in infants could heal without any complications and a growing fracture of the skull is a relatively rare complication called diastatic skull fracture. More details are found in Bilo et al. [13] which provides a review of skull fracture biomechanics as well as challenges for abuse diagnosis that pose ethical dilemmas in suspicion of child abuse.

Despite these advances, technologies providing evidence based on case-specific investigations is still not available and diagnosis of AHT is usually based on personal experiences and clinical observations mentioned above. Often, forensic investigators also refer to epidemiological studies on the diagnosis of suspected abuse [17]. However, inferring the risk of injuries based on epidemiological studies is logically flawed as many case-specific factors influence the severity of injury, e.g. age, head impact location, impact surface [21]. A more reliable biomechanically based tool providing scientific evidence for case-specific investigation is needed in the era of evidence-based medicine. A previous study presented an approach to generate subject-specific infant FE head models, which was demonstrated with newborn, 5-month and 9-month-old models. The model predictions compared well with experimental drop tests at various impact locations [41].

The objective of this study is to reconstruct two cases of suspected abuse using subject-specific infant head models, considering case-specific factors of impact locations and skull bone ossification centres based on in-depth analysis of multi-modality imaging data, together with advanced material modelling of the skull bone and soft tissues.

2. Methods

The two suspected abuse cases underwent forensic investigations in Sweden. Technical details including subject-specific FE head model generation, material modelling, determination of impact position and ossification centres are presented first, which are the basis for case reconstructions. Detailed medical records for both cases and reconstructions are presented afterwards.

2.1. FE model generation

Subject-specific FE head models for the two cases are generated based on the geometrical reconstructions of computerized tomography (CT) images following the procedures presented in a previous study [41]. The use of these anonymized CT images was approved by the local ethical committee. The resolutions of the CT images for the 3-month-old (3M) and 4-month-old (4M) are $0.32 \times 0.32 \times 0.63$ mm^3 and $0.32 \times 0.32 \times 1.5$ mm^3, respectively. For the 3M case, the CT image is corrected with a shear factor corresponding to the gantry angle of 3.5°. Afterwards, the scalp, skull, cerebrospinal fluid (CSF), brain and sutures are segmented and then smoothed out the fractures, and then three-dimensional
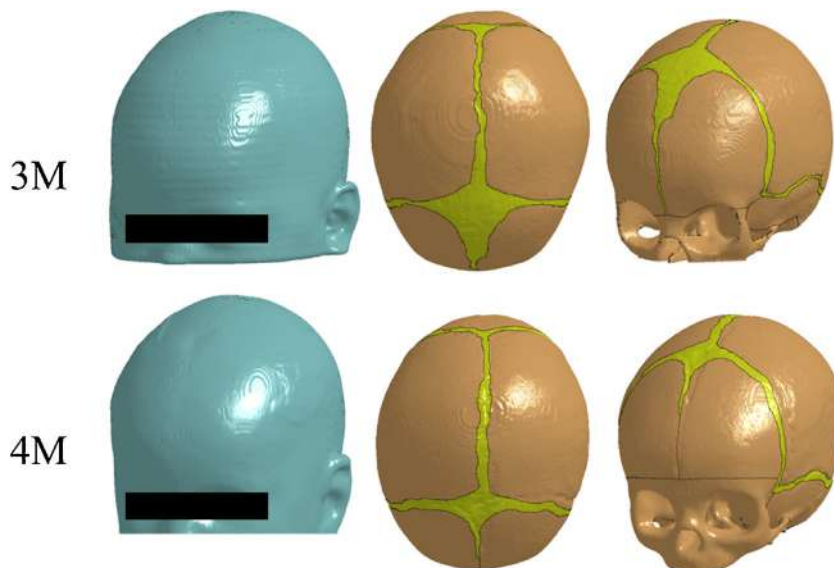
Fig. 1. Generated FE head models of the 3M (upper row) and 4M case (lower row). The skull is composed of bony plates connected by sutures and fontanels. To improve the illustration, the FE meshes are made invisible.

triangular surface meshes are generated based on the segmented images, and served as input to the software Hexotic to generate hexahedron elements. The total number of the elements in the head models is 5.68 million (Fig. 1, upper row) and 4.13 million (Fig. 1, lower row) respectively for the 3M and the 4M case. The typical element size in the skull is about 0.4 mm. All simulations are conducted with LS-Dyna 971 using an explicit dynamic solving method.

2.2. Material modelling

2.2.1. Soft tissue modelling

A 1st order Ogden hyperelastic model is used for suture accounting for the large deformation non-linear elasticity with parameters obtained by fitting the uniaxial tension stress-strain curve of infant sutures reported in Coats and Margulies [42]. The scalp model incorporates hyperplastic and viscoelastic behaviour and is modelled with two layers, representing a dense connective tissue layer and an adipose tissue layer. A Mooney–Rivlin hyperelastic model is used for dura mater, with the parameters determined from experimental tests of fetal dura mater [43].

The above nonlinear models for the suture, scalp, and dura based on experimental data enable infant head models to predict acceleration–time curves and impact surface area that are comparable with experimental findings at various impact locations [41] and a detailed description for the choice of material properties is found therein. A summary of the material properties used for the soft tissues in the 3M and 4M head models is listed in Table 1.

2.2.2. Skull bone modelling

The skull bones are modelled with orthotropic material accounting the grain fibers radiating from the ossification centres of each bone plate estimated according to their anatomical locations (Fig. 5). Dramatic changes in grain fibre patterns have been demonstrated during early infancy – from clearly visible in newborns [20,42,44] to almost invisible already in six-month-olds [45], corresponds to a high anisotropy ratio in newborn to 1.25 in 6-year-olds and becomes isotropic in adults. The structural changes are accompanied by mechanical properties changes – a decrease with anisotropy and an increase in stiffness, ranging from a few hundred MPa in infants up to several GPa in 6-year-olds. In a previous work, we have developed an approach for obtaining age-dependent skull bone orthotropic parameters based on experimental data reflecting the two biological growth factors. The same procedure was used for determining the 3M and 4M skull bone Young's modulus with detailed steps and relevant references provided therein [41]. Its effectives have been demonstrated in infant head models from newborn to 9-month-old subjected to impacts at different locations as well as compression test. Using the derived results, the skull bone material properties are presented in Tables 2 and 3 for the two cases, where E_1 is the Young's modulus along the parallel-to-fibre direction and E_2 is perpendicular-to-fibre direction.

Skull fracture was not accounted in the previous models due to the low drop height from 30 cm [41] unlikely to cause skull fractures. At higher impact height, fracture occurs when the stress in the skull exceeds the ultimate stress. In the experimental study by Coats and Margulies [42], besides the Young's modulus, the ultimate stress was also measured in infant skull bones from 23 calvaria (21-week gestation to 13 months old) under high strain rate showing a stiffer bone in general has a higher ultimate stress (Fig. 2). The elastic modulus (E_2) and the paired ultimate stress for the parietal and occipital bone are plotted and regressed with a linear model, resulting coefficient of determination $R^2 = 0.59$ and 0.56 for the parietal and occipital bone respectively. The same regressed linear model is also used for the other parallel-to-fibre direction. Based on the regressed model, the ultimate stress values obtained corresponding to elastic modulus is listed in Tables 2 and 3.

2.3. Determination of impact location

For the 3M case, both T1 weighted MRI and CT images are available. The MRI images show two spots of scalp bruising (Fig. 3a, left), which are rigidly registered to the CT image based on which the FE mesh is generated (Fig. 3a, right). Two scalp bruising positions are identified and the one at the upper left is most plausible due to another fracture near the skull base at the same side (Fig. 3b).

For the 4M case, to determine the maximum scalp swelling location, a healthy head image was recovered by flipping the left non-injured side to the right side. Then a nonlinear image registration using Diffeomorphic Demons (DD) algorithm was performed to quantify the displacement field of the outer scalp surface from healthy to injured state. The displacement field of the scalp surface is shown in Fig. 4 with the red colour indicating the maximum swelling point. The same procedure was used to quantify brain swelling in an earlier study with detailed information provided therein [46,47]. The results indicated two locations with largest swelling that are above 12 mm. By further analysis using the brain injury information of the haemorrhage shape, the posterior swelling point is identified as the most plausible impact location (Fig. 4).

2.4. Ossification centres in the infant skull

The ossification centers located at the respective eminences, which are calculated as the largest Gaussian curvature for the reconstructed triangular skull surfaces at each point using the angle deficit method (Fig. 5). Despite some artifacts, the ossification centers are well identifiable by using anatomical illustrations as prior knowledge. The obtained centers are then prescribed to the skull bone for orthotropic material modelling.

2.5. Medical records and reconstruction

2.5.1. 3M case

The 3-month-old girl entered the emergency department with immediate posttraumatic symptoms of vomiting, excitation and right sided eye deviation and nystagmus. No detectable external

Table 1
Summary of material properties for the infant head model.

Tissue	Material constants	Density (kg/m³)	Poisson's ratio
Brain	$\mu_1 = 53.8\,Pa, \alpha_1 = 10.1,\ \mu_2 = -120.4\,Pa,\ \alpha_2 = -12.9$	1040.0	~0.5
CSF	$K = 2.1\,GPa$	1000.0	0.5
Suture	$\mu_1 = 1.48 \times 10^4\,Pa,\ \alpha_1 = 6.9$	1133.0	0.499
Scalp connective tissue	$\mu_1 = 1.30 \times 10^4\,Pa,\ \alpha_1 = 24.2$	1133.0	~0.5
Scalp adipose tissue	$\mu_1 = 3.99 \times 10^3\,Pa,\ \alpha_1 = 8.8$	1133.0	~0.5
Dura mater	Mooney–Rivlin model $C_1 = 1.18\,MPa, C_2 = 0.295\,MPa$	1133.0	0.49

Table 2
Material properties and parameters in the 3M infant head.

Property	Parietal	Occipital
Density (kg/m^3)	$\rho = 2083$	$\rho = 2083$
Young's modulus (MPa)	$E_1 = 830.4$, $E_2 = E_3 = 466.1$	$E_1 = 626.5$, $E_2 = E_3 = 343.3$
Poisson's ratio	$v_{21} = v_{31} = 0.12$, $v_{32} = 0.19$	$v_{21} = v_{31} = 0.12$, $v_{32} = 0.19$
Shear modulus (MPa)	$G_{12} = G_{31} = 267.0$, $G_{23} = 195.8$	$G_{12} = G_{31} = 199.4$, $G_{23} = 144.2$
Tensile strength (MPa)	$S_{1T} = 51.4$ (40.6), $S_{2T} = 30.5$ (23.9)	$S_{1T} = 23.2$ (18.8), $S_{2T} = 15.1(12.2)$
Compressive strength (MPa)	$S_{2C} = 40.7$ (31.9)	$S_{2C} = 20.2$ (16.2)
Normal strength (MPa)	$S_N = 30.5$ (23.9)	$S_N = 15.1$ (12.2)
Shear strength (MPa)	$S_{12} = S_{31} = 16.5(13.1)$, $S_{23} = 12.8$ (10.1)	$S_{12} = S_{31} = 7.4$ (6.0), $S_{23} = 6.4$ (5.1)

Note: Two simulations are performed for the 3M case using both the bassline and the 95% PI lower strength values (in the bracket) calculated according to the regressed linear equation (Fig. 2).

Table 3
Material properties and parameters in the 4M infant head.

Property	Parietal	Occipital
Density (kg/m^3)	$\rho = 2082$	$\rho = 2082$
Young's modulus (MPa)	$E_1 = 840.2$, $E_2 = E_3 = 499.1$	$E_1 = 639.3$, $E_2 = E_3 = 368.9$
Poisson's ratio	$v_{21} = v_{31} = 0.13$, $v_{32} = 0.19$	$v_{21} = v_{31} = 0.13$, $v_{32} = 0.19$
Shear modulus (MPa)	$G_{12} = G_{31} = 276.8$, $G_{23} = 209.7$	$G_{12} = G_{31} = 208.0$, $G_{23} = 155.0$
Tensile strength (MPa)	$S_{1T} = 52.0$, $S_{2T} = 32.4$	$S_{1T} = 23.6$, $S_{2T} = 15.8$
Compressive strength (MPa)	$S_{2C} = 43.2$	$S_{2C} = 21.1$
Normal strength (MPa)	$S_N = 32.4$	$S_N = 15.8$
Shear strength (MPa)	$S_{12} = S_{31} = 17.1, S_{23} = 13.6$	$S_{12} = S_{31} = 7.7$, $S_{23} = 6.7$

Note: Baseline strength values are calculated from the regressed linear equation (Fig. 2).
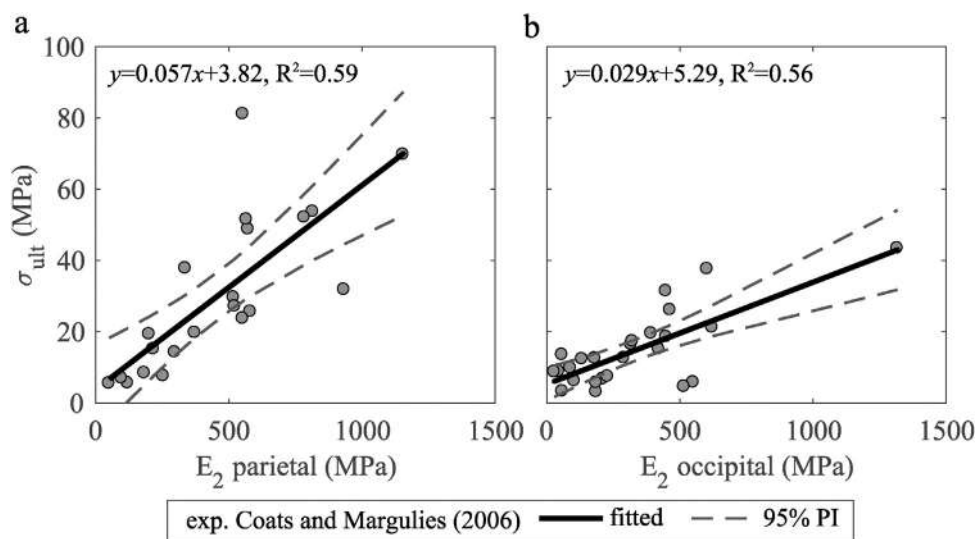
**Fig. 2.** The elastic modulus in the perpendicular-to-fibre direction (E_2) and the paired ultimate stress is regressed with a linear model (referred to as the bassline) for the parietal (left) and occipital bone (right). The dashed curve represents the 95% prediction interval (PI) for the regression curve.

signs of trauma were observed on head, neck or overall body immediately after the trauma. Initial CT scan of the head showed no haemorrhage but extensive low attenuating area over parietal and occipital lobes bilaterally, interpreted as signs of oedema/hypoxia. Lumbar puncture showed clear CSF and fundoscopic exam showed no signs of retinal bleedings. Structural MRI image of the head taken one day post trauma showed no haemorrhage but right occipital and superior frontal temporal interpreted as cytotoxic oedema. MR-angiography taken the same time showed no vascular aberrations. Full skeletal survey performed one day

post trauma was also normal. The infant was born premature at gestational age of week 35 under uncomplicated partus, weighting 2.41 kg at birth.

In particular, the reconstructed surface from CT scan showed undislocated fracture of parietal bones at both sides crossing the sagittal suture, approximately 6 cm in the right, and about 3 cm in the left. The extent of the skull fractures and other circumstances initiated a police investigation of suspected child abuse. The mother who was taking care of the child claimed the infant had fallen from her arm at the residence from an estimated height of
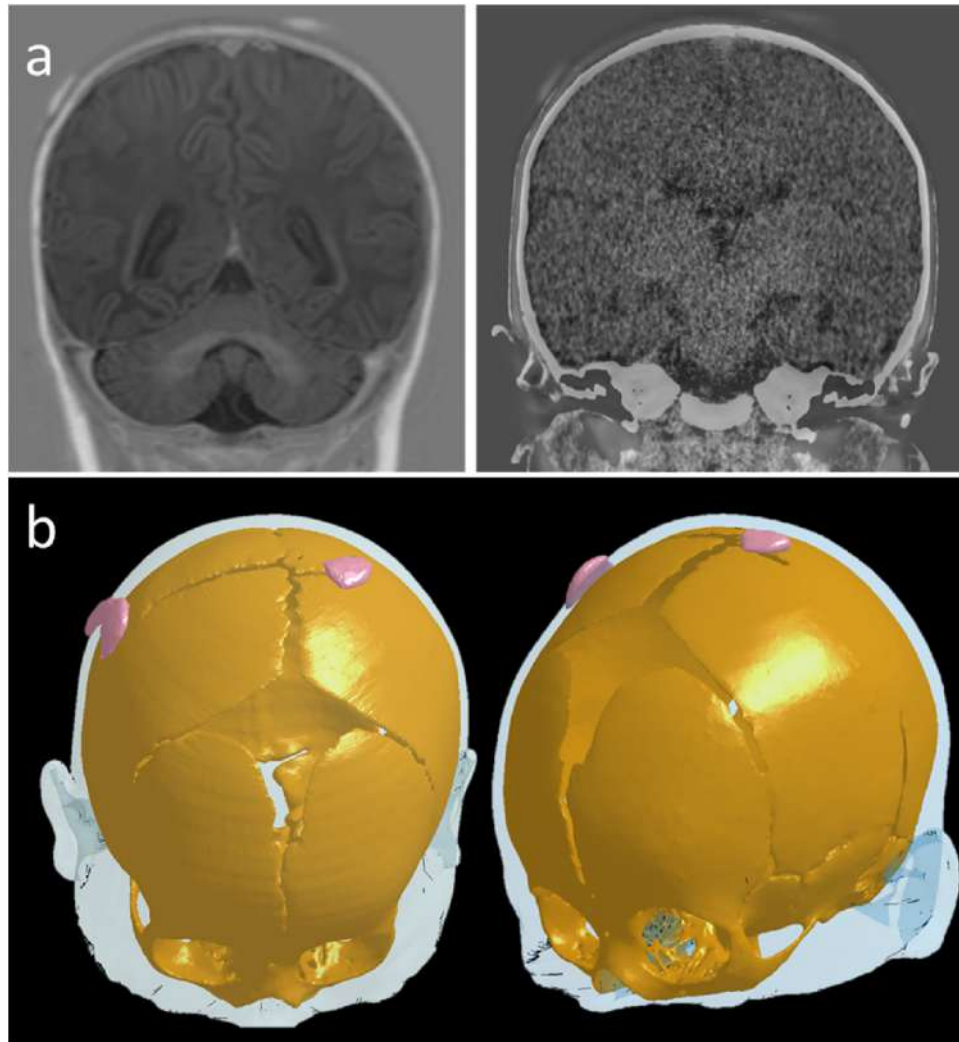
Fig. 3. Determination of impact locations based on the bruising of scalp. (a) A coronal section of the T1 MRI image (left) is rigidly aligned to the CT image (right). (b) The identified scalp swelling locations are imported to the reconstructed skull surface from the CT image (sharing the same coordinate as the FE model) to guide the rotation of the head model prior to impact.

0.84, possibly impacted to a dog bed (Fig. 6a). An examination of the dog bed showed it did not seem to offer any protection due to its thin structure. Numerical simulation of free fall is performed by prescribing an initial velocity corresponding to the estimated height to the head model to impact at the identified location as detailed in previous sections (Fig. 6b,c).

2.5.2. 4M case

For the 4M case, the caretaker claimed the infant had fallen from a baby changing table onto the floor made of linoleum flooring over concrete at an estimated height of 1.1 m (Fig. 7a). The boy had initial scream but was conscious. A first examination in hospital showed large volume of swollen hematoma ($10 \times 5 \times 1.5$ cm^3) in the right parietal area. A later acute CT-scan of brain without contrast showed intraparenchymal bleeding in the right parietal area (3.1×3.5 cm^2) in the axial plane with perifocal oedema noted. Multiple fractures were noted in the frontal and parietal bones in addition to an impression fracture with 3 mm diastasis and intermedial fragment. Midline structures were shifted 0.3 cm to the left and the right posterior horn of the lateral ventricle was compressed. Subarachnoid bleeding was seen at the right parietal and occipital lobes as well as at interhemispheric fissure. A massive extracranial hematoma

about 1.7 cm wide was seen at frontoparietal area. The 4-month-old boy was born in due at a gestational age of week 42, uncomplicated delivery with a full APGAR score, weighting 4.01 kg at 12 days postpartum.

Due to deteriorating consciousness, an acute neurosurgical intervention was performed. During surgery, a large rift was seen in the dura at the site where the skull fractured and bleeding from the cortical laceration was seen. The hematoma cavity was evacuated before skull bone fragments were put together. Preoperative laboratory data on hemostasis were within normal range. Fundoscopic exam and full skeletal survey did not show abnormal. Postoperative intensive care and neurological complications were related to bleeding and neurosurgery as anticipated.

Reconstructed skull surface from CT images showed fracture in the parietal bone, but not seen in the frontal bone as noted in the medical record. The treating medical doctor stated "this has to be abuse", which initiated a police investigation followed by forensic examination. Numerical simulation of free fall is performed by prescribing an initial velocity corresponding to the estimated height of 1.1 m to the model to impact at the identified location as detailed in previous sections (Fig. 7).
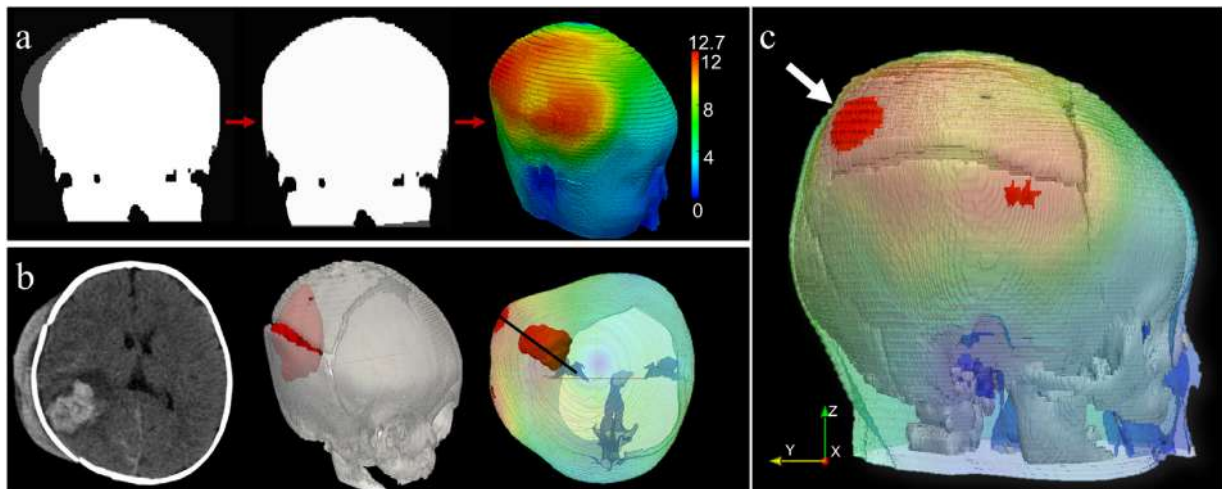
Fig. 4. (a) The segmented head binary image masks from the recovered healthy and the injured CT image were rigidly aligned first (left), and then served as input for DD registration from which displacement fields were obtained. After DD registration, the discrepancy becomes nearly invisible between the overplayed images, indicating a good alignment (middle). From the DD registration, a three-dimensional displacement field was obtained that represents the scalp swelling magnitude from healthy to injured state (right). (b) An axial CT slice shows brain haemorrhage (left) which was segmented manually and overlaid with the reconstructed skull surface (middle). Viewing from above, the maximum direction of the haemorrhage volume is perpendicular to the posterior swelling point, suggesting it to be the most likely impact location (c) and is isolated to be imported into the FE model to guide the rotation of the head model prior to impact.
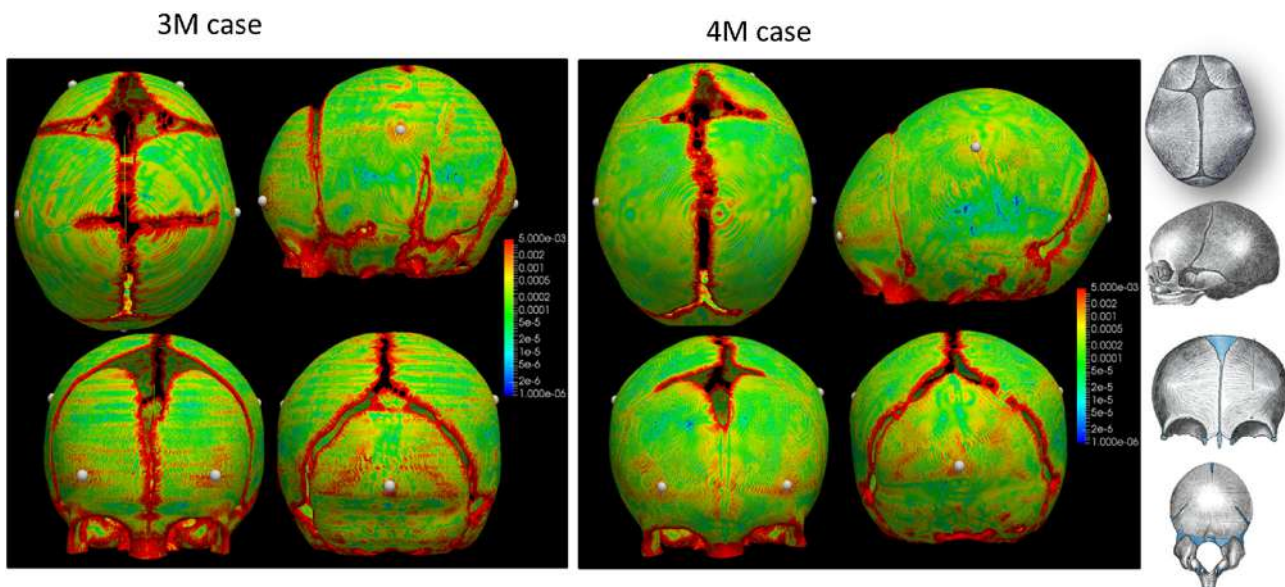
Fig. 5. Gaussian curvatures calculated for the skull bone surfaces reconstructed from CT images for the 3M (left) and 4M (right). The ossification centres for each bone plates are identified as the maximum curvature together with anatomical illustrations by Gray [48] as prior knowledge. The obtained centres are indicated as white dots.

3. Results

The reconstructed results for the 3M case showed small fracture crossed the sutures using baseline strength values (Fig. 8b). The same model when using the 95% PI lower strength values, showed large fractures crossing the suture at both sides of the skull (Fig. 8c), resembling the observed fractures in the CT images (Fig. 8a). There are also a few smaller predicted fractures from the model which are not seen in the CT images indicated with light colored lines.

The 4M model predicted a large fracture from the back to front lines with similar size as in the CT image. However, a concave fracture is predicted as opposed to a convex shape seen in the CT image. A few small linear fractures are also seen despite not shown in the CT image (Fig. 9).

4. Discussion

Both cases were initially suspected to abuse and the central question during the diagnosis is: can the provided history explain the observed fractures? Our analyses reveal in both cases, the injury patterns including fracture crossing the suture and multiple fractures could be possible due to a simple fall. The results from this biomechanical investigation were provided to the forensic investigation team and aided their decision-making for both cases.

For the reconstruction, special care is taken for determining the impact location which has a substantial influence on the global head response, and consequently the predicted skull fractures [41] attributing to the special structural characteristics of infant skull composed of flexible plates. Therefore, a proper estimation of the impact location is crucial for a reliable prediction of skull fractures.
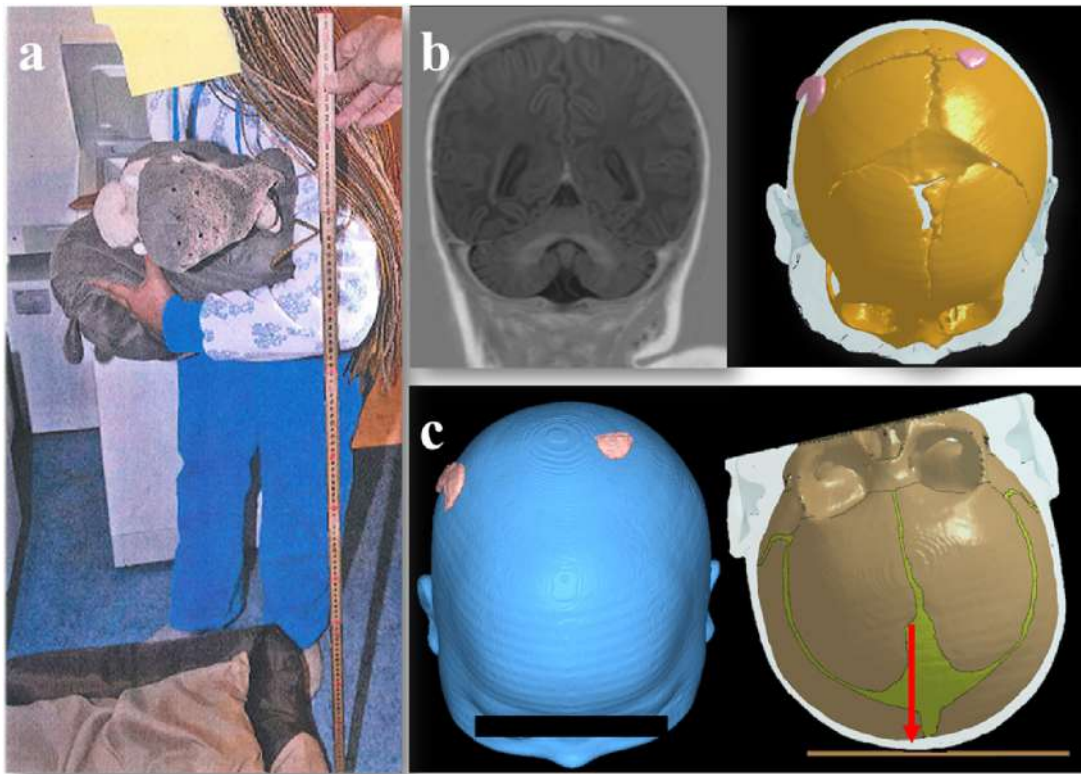
Fig. 6. Analyse and reconstruction of the 3M case. (a) Estimation of the drop height (0.84 m) according to the mother who described the infant had fallen from her arm. (b) Reconstructed surfaces of the skull and the scalp bruising from the T1 MRI images showing the two possible impact locations. (c) The estimated impact locations were imported into the FE model to guide the rotation of the model to impact at the identified upper swelling point.
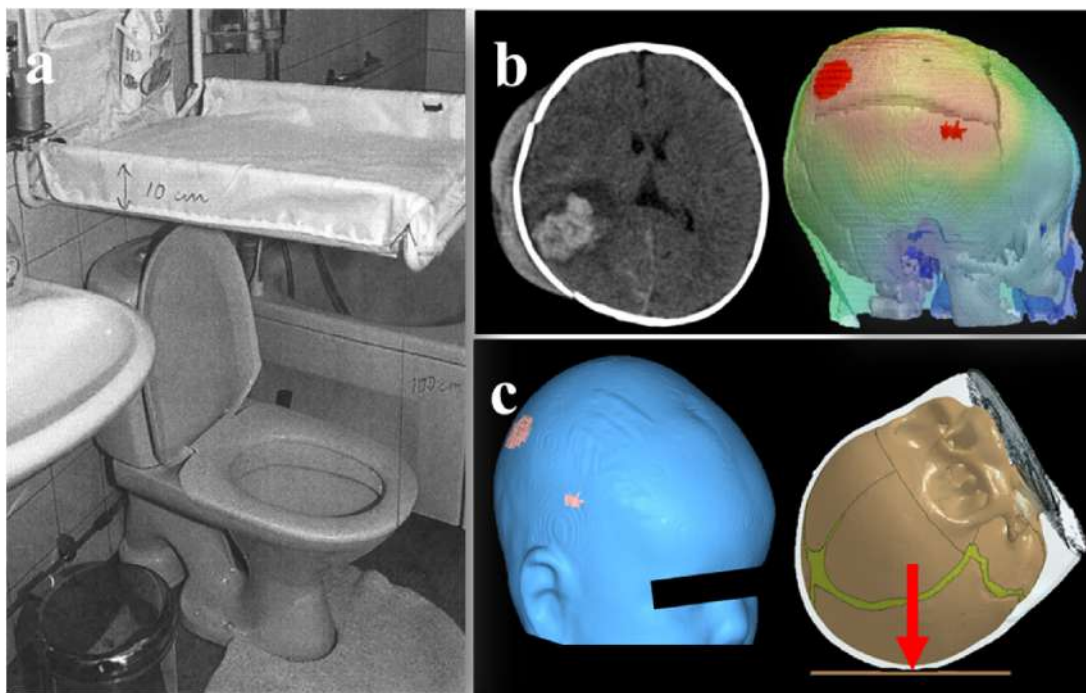
Fig. 7. Analyse and reconstruction of the 4M case. (a) Estimation of the maximum vertical drop height and impact velocity. (b) Estimation of possible impact points according to the maximum swelling point identified by image registration and the brain tissue haemorrhage shape. (c) The estimated impact points were imported into the FE model to guide the model the rotation of the model to impact at the identified location on the upper, back swelling point with a vertical drop of 1.1 m.
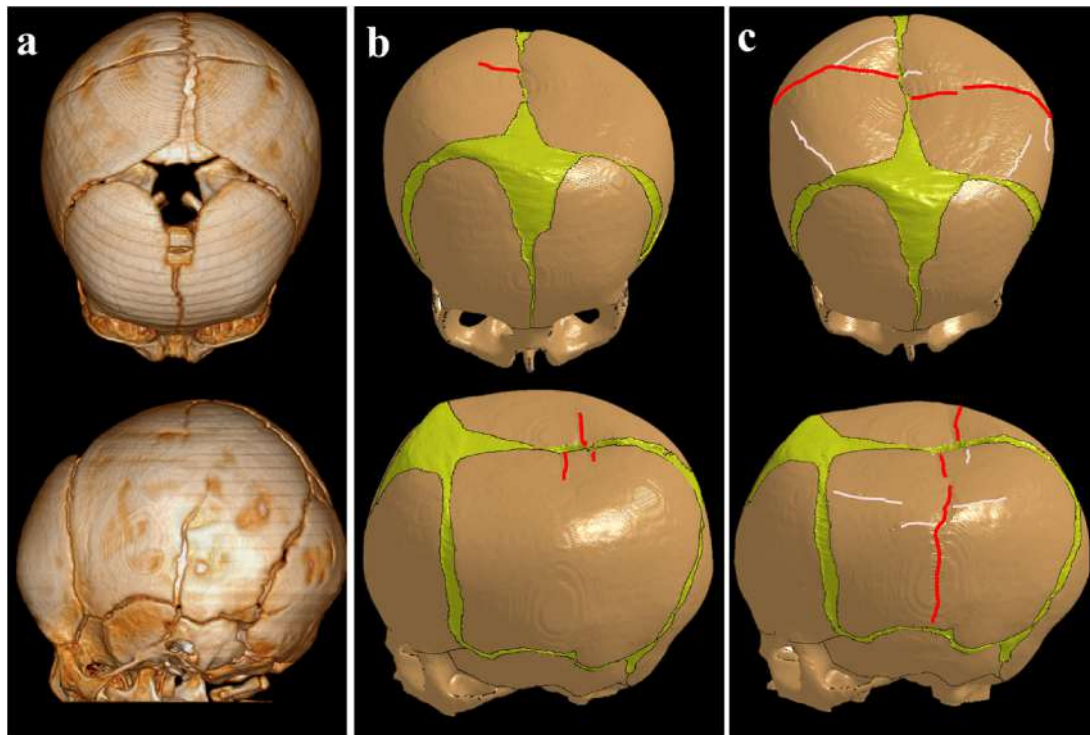
Fig. 8. Analyse results of the 3M case. (a) Skull fractures shown from the reconstructed surfaces of the CT scans. Predicted skull fractures from the 3M model captured from different views using baseline strength values (b) and 95% PI lower strength values (c).
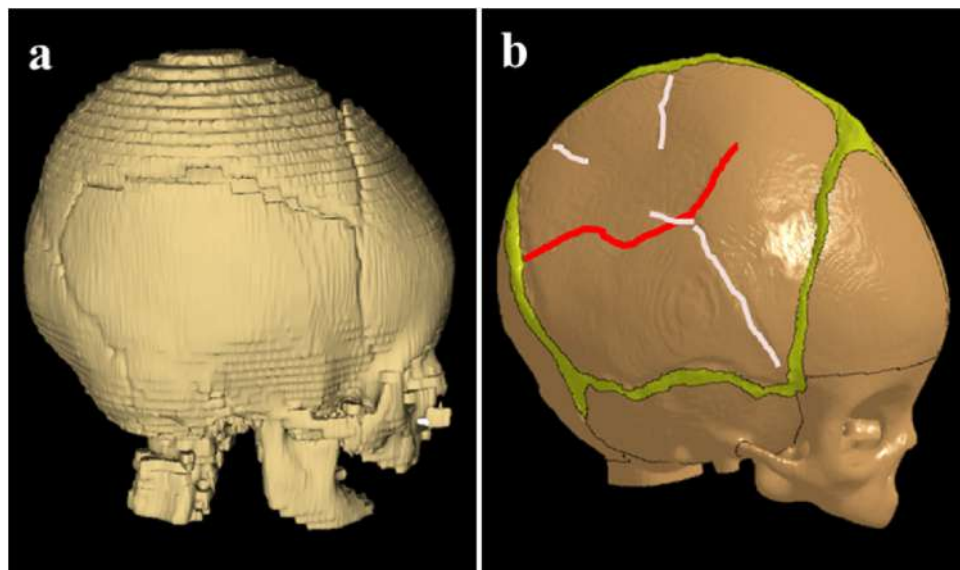
Fig. 9. Analyse results of the 4M case. (a) Skull fractures shown from the reconstructed surfaces of the CT scans. (b) Predicted skull fractures form the 4M model.

Maximum swelling point from the scalp has been previously used as the impact location in bicycle accident reconstructions [49,50]. Indeed, there is a high likelihood that the scalp swelling occurs at the impact locations for a direct impact, but the swelling scalp can also be caused by a secondary injury due to the fractured skull. Further, when the surface area of contact is large, soft-tissue injury at the cranial impact site may be minimal or absent [51] making it difficult to identify the impact location. In this study, impact locations are identified based on multimodality imaging data instead of purely relying on the maximum scalp swelling. The impact location for the 3M case is determined by combining CT and

MRI images (Fig. 3). While for the 4M case, besides the maximum scalp swelling, the shape of intracranial haemorrhage provides further aid to locate the most plausible impact location (Fig. 4). For each case, of the two identified impact locations, one is chosen as impact location while the other could be explained as secondary injury due to the fractured skull.

In newborns, the skull has a visible fiber orientation radiating from the ossification centers [20,42]. The fibers causes the infant skull to behave anisotropically as confirmed by experimental studies [44,52], being stiffer along the fiber direction compared with perpendicular directions. Because of this, fracture lines in the

infant skull usually follow along the spiculae emanating from centers of ossification as observed in PMHS [20]. The fracture patterns in the experimental studies using human PMHS [20,24] as well as a series of animal experimental studies using piglets' heads [53] also suggested the skull bones are easier to fracture parallel to the spiculae, than run across them. To incorporate the direction-specific material properties, ossification centers are obtained by combining skull surface curvatures with anatomical illustrations (Fig. 5) which are shown to give a reasonable estimation before new approaches emerge.

The subject-specific FE head models allow considering accurate geometry of the suture and skull of the two cases evaluated, together with special efforts on determination of impact points and ossification centers, the predicted skull fracture patterns overall correlates with the CT images. Nevertheless, a number of modeling uncertainties exist; in particular skull bone material properties (both elastic modulus and failure stress) influence the fracture patterns. The skull bone material properties are estimated from literature inferred from specimens at a similar age which does not allow incorporating subject-specific information especially infants with Vitamin D deficiency are likely to have a higher risk of skull fracture [2]. Any or a combination of above factors could have led to the small fractures predicted from the model but not seen in real cases, as well as the predicted fracture patterns. In the future, when techniques are available to account for more detailed and accurate subject-specific information e.g. skull bone properties determined using advanced micro-CT images, different types of ossification (e.g. endochondral versus intramembranous), will further advance the prediction of infant skull fractures. Therefore, at this current stage, the simulation results need to be interpreted with caution especially when providing such evidence to the authorities for diagnosis of abuse, acknowledging the limitations and uncertainties. Nevertheless, it represents one step further to advance the diagnosis with case-specific biomechanical evidence which we believe are important to move one step forward allowing to protect the most vulnerable children and also to reduce the number of wrongful convictions of innocent parents/caretakers and may have enormous medico-legal implications world-wide.

Author contributions

Xiaogai Li: Conceptualization, Methodology, Formal analysis, Writing — Original Draft, Funding Acquisition.

Håkan Sandler: Conceptualization, Resources, Writing — Review & Editing, Funding Acquisition.

Svein Kleiven: Conceptualization, Methodology, Writing — Review & Editing, Funding Acquisition.

Acknowledgements

References

[1] C.J. Meservy, R. Towbin, R.L. McLaurin, P.A. Myers, W. Ball, Radiographic characteristics of skull fractures resulting from child abuse, Am. J. Roentgenol. 149 (1987) 173–175.

[2] E.G. Flaherty, J.M. Perez-Rossello, M.A. Levine, W.L. Hennrikus, C.W. Christian, et al., Evaluating children with fractures for child physical abuse, Pediatrics 133 (2014) e477–e489.

[3] W. Weber, Biomechanical fragility of the infant skull, Z. Rechtsmed. 94 (1985) 93–101.

[4] S.E. Parks, J.L. Annest, H.A. Hill, D.L. Karch, Pediatric abusive head trauma: recommended definitions for public health surveillance and research, Centers for Disease Control and Prevention, Atlanta, GA, 2012, pp. 5–16.

[5] M. Colbourne, Abusive head trauma: evolution of a diagnosis, B. C. Med. J. 57 (2015) 331–335.

[6] T. Hinds, E. Shalaby-Rana, A.M. Jackson, Z. Khademian, Aspects of abuse: abusive head trauma, Curr. Probl. Pediatr. Adolesc. Health Care 45 (2015) 71–79.

[7] American Academy of Pediatrics, Statement on abusive head trauma (Shaken Baby Syndrome), (2017) (Accessed 9, April 2017). https://www.aap.org/en-us/about-the-aap/aap-press-room/aap-press-room-media-center/Pages/Abusive-Head-Trauma-Fact-Sheet.aspx..

[8] A.H. Ross, S.M. Abel, D. Radisch, Pattern of injury in child fatalities resulting from child abuse, Forensic Sci. Int. 188 (2009) 99–102.

[9] W.J. King, M. MacKay, A. Sirnick, Group CSBS, et al., Shaken baby syndrome in Canada: clinical characteristics and outcomes of hospital cases, CMAJ 168 (2003) 155–159.

[10] X. Fang, D.S. Brown, C.S. Florence, J.A. Mercy, The economic burden of child maltreatment in the United States and implications for prevention, Child Abuse Negl. 36 (2012) 156–165.

[11] C. Peterson, L. Xu, C. Florence, S.E. Parks, T.R. Miller, et al., The medical cost of abusive head trauma in the United States, Pediatrics 134 (2014) 91–99.

[12] C. Jenny, K.P. Hymel, A. Ritzen, S.E. Reinert, T.C. Hay, Analysis of missed cases of abusive head trauma, JAMA 281 (1999) 621–626.

[13] R.A. Bilo, S.G. Robben, R.R. Rijn, Forensic aspects of pediatric fractures: differentiating accidental trauma from child abuse, Springer Science & Business Media, 2010.

[14] R.E. Helfer, T.L. Slovis, M. Black, Injuries resulting when small children fall out of bed, Pediatrics 60 (1977) 533–535.

[15] A.K. Thompson, G. Bertocci, W. Rice, M.C. Pierce, Pediatric short-distance household falls: biomechanics and associated injury severity, Accid. Anal. Prev. 43 (2011) 143–150.

[16] J.M. Leventhal, K.D. Martin, A.G. Asnes, Fractures and traumatic brain injuries: abuse versus accidents in a US database of hospitalized children, Pediatrics 126 (2010) e104–e115.

[17] J.P. Ehsani, J.E. Ibrahim, L. Bugeja, S. Cordner, The role of epidemiology in determining if a simple short fall can cause fatal head injury in an infant: a subject review and reflection, Am. J. Forensic Med. Pathol. 31 (2010) 287–298.

[18] C. Jenny, K.P. Hymel, N. Rangarajan, Biomechanics of pediatric head injury, in: K.A. Collins, R.W. Byard (Eds.), Forensic pathology of infancy and childhood, Springer-Verlag, New York, 2014, pp. 435–453.

[19] K.P. Hymel, D.F. Willson, S.C. Boos, D.A. Pullin, K. Homa, et al., Derivation of a clinical prediction rule for pediatric abusive head trauma, Pediatr. Crit. Care Med. 14 (2013) 210–220.

[20] P. Holck, What can a baby's skull withstand? Testing the skull's resistance on an anatomical preparation, Forensic Sci. Int. 151 (2005) 187–191.

[21] A. Hamel, M. Llari, M.D. Piercecchi-Marti, P. Adalian, G. Leonetti, et al., Effects of fall conditions and biological variability on the mechanism of skull fractures caused by falls, Int. J. Leg. Med. 127 (2013) 111–118.

[22] C.J. Hobbs, Skull fracture and the diagnosis of abuse, Arch. Dis. Child. 59 (1984) 246–252.

[23] P.K. Kleinman, Diagnostic imaging of child abuse, Cambridge University Press, 2015.

[24] W. Weber, Experimental studies of skull fractures in infants, Z. Rechtsmed. 92 (1984) 87–94.

[25] T.S. Deland, E. Niespodziewanski, T.W. Fenton, R.C. Haut, The role of interface on the impact characteristics and cranial fracture patterns using the immature porcine head model, J. Forensic Sci. (2016) 61.

[26] B.J. Powell, T.G.Baumer, N.V. Passalacqua, C.D. Wagner, R.C. Haut, et al. Forensic pathology tool to predict pediatric skull fracture patterns. National Institute of Justice Grant 2007-DN-BX-K196 Final Report; 2012.

[27] B.J. Powell, N.V. Passalacqua, T.W. Fenton, R.C. Haut, Fracture characteristics of entrapped head impacts versus controlled head drops in infant porcine specimens, J. Forensic Sci. 58 (2013) 678–683.

[28] P.E. Vaughan, C. Vogelsberg, J.M. Vollner, T.W. Fenton, R.C. Haut, The role of interface shape on the impact characteristics and cranial fracture patterns using the immature porcine head model, Forensic Sci. Int. 61 (2016) 1190–1197.

[29] R.C. Haut, F. Wei, Biomechanical studies on patterns of cranial bone fracture using the immature porcine model, J. Biomech. Eng. 139 (2017) 021001.

[30] H. von Holst, X. Li, Numerical impact simulation of gradually increased kinetic energy transfer has the potential to break up folded protein structures resulting in cytotoxic brain tissue edema, J. Neurotrauma 30 (2013) 1192–1199.

[31] C. Giordano, S. Kleiven, Connecting fractional anisotropy from medical images with mechanical anisotropy of a hyperviscoelastic fibre-reinforced constitutive model for brain tissue, J. R. Soc. Interface 11 (2014) 20130914.

[32] S. Kleiven, Predictors for traumatic brain injuries evaluated through accident reconstructions, Stapp. Car Crash J. 51 (2007) 81–114.

[33] C. Giordano, X. Li, S. Kleiven, Performances of the PIPER scalable child human body model in accident reconstruction, PLoS One 12 (2017)e0187916.

[34] P. Beillas, C. Giordano, V. Alvarez, X. Li, X. Ying, et al., Development and performance of the PIPER scalable child human body models, 14th International Conference on the Protection of Children in Cars (2016) 19.

[35] J. Ho, Z. Zhou, X. Li, S. Kleiven, The peculiar properties of the falx and tentorium in brain injury biomechanics, J. Biomech. 60 (2017) 243–247.

[36] X. Li, X.L. Gao, S. Kleiven, Behind helmet blunt trauma induced by ballistic impact: a computational model, Int. J. Impact Eng. 91 (2016) 56–67.

[37] Z. Li, W. Liu, J. Zhang, J. Hu, Prediction of skull fracture risk for children 0–9 months old through validated parametric finite element model and cadaver test reconstruction, Int. J. Leg. Med. 129 (2015) 1055–1066.

[38] B. Coats, S.S. Margulies, S. Ji, Parametric study of head impact in the infant, Stapp. Car Crash J. 51 (2007) 1–15.

[39] S. Sullivan, B. Coats, S.S. Margulies, Biofidelic neck influences head kinematics of parietal and occipital impacts following short falls in infants, Accid. Anal. Prev. 82 (2015) 143–153.

[40] C. Hobbs, ABC of child abuse. Fractures, BMJ: Br. Med. J. 298 (1989) 1015.

[41] X. Li, H. Sandler, S. Kleiven, The importance of nonlinear tissue modelling in finite element simulations of infant head impacts, Biomech. Model Mechanobiol. 16 (2017) 823–840.

[42] B. Coats, S.S. Margulies, Material properties of human infant skull and suture at high rates, J. Neurotrauma 23 (2006) 1222–1232.

[43] D.I. Bylski, T.J. Kriewall, N. Akkas, J.W. Melvin, Mechanical behavior of fetal dura mater under large deformation biaxial tension, J. Biomech. 19 (1986) 19–26.

[44] G.K. McPherson, T.J. Kriewall, The elastic modulus of fetal cranial bone: a first step towards an understanding of the biomechanics of fetal head molding, J. Biomech. 13 (1980) 9–16.

[45] S.S. Margulies, K.L. Thibault, Infant skull and suture properties: measurements and implications for mechanisms of pediatric brain injury, J. Biomech. Eng. 122 (2000) 364–371.

[46] X. Li, H. von Holst, S. Kleiven, Decompressive craniectomy causes a significant strain increase in axonal fiber tracts, J. Clin. Neurosci. 20 (2013) 509–513.

[47] H. von Holst, X. Li, S. Kleiven, Increased strain levels and water content in brain tissue after decompressive craniotomy, Acta Neurochir. 154 (2012) 1583–1593.

[48] H. Gray, Anatomy of the human body, Lea & Febiger, 1918.

[49] M. Fahlstedt, B. Depreitere, P. Halldin, J. Vander Sloten, S. Kleiven, Correlation between injury pattern and finite element analysis in biomechanical reconstructions of traumatic brain injuries, J. Biomech. 48 (2015) 1331–1335.

[50] A. Post, T.B. Hoshizaki, M.D. Gilchrist, S. Brien, M. Cusimano, et al., Traumatic brain injuries: the influence of the direction of impact, Neurosurgery 76 (2015) 81–91.

[51] D. Arnholz, K.P. Hymel, T.C. Hay, C. Jenny, Bilateral pediatric skull fractures: accident or abuse? J. Trauma Acute Care Surg. 45 (1998) 172–174.

[52] T.J. Kriewall, Structural, mechanical, and material properties of fetal cranial bone, Am. J. Obstet. Gynecol. 143 (1982) 707–714.

[53] T.G. Baumer, N.V. Passalacqua, B.J. Powell, W.N. Newberry, T.W. Fenton, et al., Age-dependent fracture characteristics of rigid and compliant surface impacts on the infant skull — A porcine model, J. Forensic Sci. 55 (2010) 993–997.